END
DATE
FILMED

11 —79

DDC

AD A075285

FATIGUE MICROCRACK BEHAVIOR UNDER THE INFLUENCE OF SURFACE RESIDUAL STRESSES
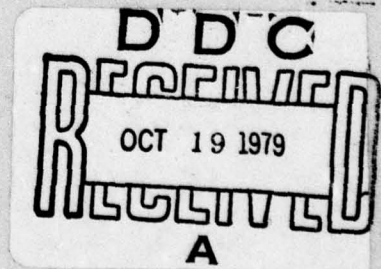
J. E. Hack and G. R. Leverant
Southwest Research Institute
P.O. Drawer 28510
San Antonio, Texas 78284

INTERIM REPORT for Period August 1, 1978 - July 31, 1979
Contract N00014-78-C-0674

Prepared for
OFFICE OF NAVAL RESEARCH
800 North Quincy Street
Arlington, Virginia
22217

October 1, 1979

NR 031-812

SOUTHWEST RESEARCH INSTITUTE
SAN ANTONIO   HOUSTON

UNCLASSIFIED

SECURITY CLASSIFICATION OF THIS PAGE *(When Data Entered)*

REPORT DOCUMENTATION PAGE	READ INSTRUCTIONS BEFORE COMPLETING FORM

1. REPORT NUMBER	2. GOVT ACCESSION NO.	3. RECIPIENT'S CATALOG NUMBER
Interim Rept. 1 Aug 78-31 Jul 79		

4. TITLE *(and Subtitle)*	5. TYPE OF REPORT & PERIOD COVERED
FATIGUE MICROCRACK BEHAVIOR UNDER THE INFLUENCE OF SURFACE RESIDUAL STRESSES	Interim Report August 1, 1978 – July 31, 1979
	6. PERFORMING ORG. REPORT NUMBER 02-5382

7. AUTHOR(s)	8. CONTRACT OR GRANT NUMBER(s)
J. E. Hack G. R. Leverant	N00014-78-C-0674

9. PERFORMING ORGANIZATION NAME AND ADDRESS	10. PROGRAM ELEMENT, PROJECT, TASK AREA & WORK UNIT NUMBERS
Southwest Research Institute P. O. Drawer 28510 San Antonio, Texas 78284	Project Element 122201 NR 031-812/6-23-78 (471)

11. CONTROLLING OFFICE NAME AND ADDRESS	12. REPORT DATE
Office of Naval Research 800 North Quincy Street Arlington, Virginia 22217	October, 1979
	13. NUMBER OF PAGES 33 + Prelims

14. MONITORING AGENCY NAME & ADDRESS*(if different from Controlling Office)*	15. SECURITY CLASS. *(of this report)*
	UNCLASSIFIED
	15a. DECLASSIFICATION/DOWNGRADING SCHEDULE

16. DISTRIBUTION STATEMENT *(of this Report)*

Reproduction in whole or in part is permitted for any purpose of the United States Government. Distribution is unlimited.

17. DISTRIBUTION STATEMENT *(of the abstract entered in Block 20, if different from Report)*

18. SUPPLEMENTARY NOTES

DDC

RECEIVED OCT 19 1979

A

19. KEY WORDS *(Continue on reverse side if necessary and identify by block number)*

Fatigue
Microcrack
Residual Stress
Titanium
Surface Crack Opening Displacement
Stress Intensity

20. ABSTRACT *(Continue on reverse side if necessary and identify by block number)*

Direct observations of the surface crack opening displacement (SCOD) of surface microcracks have been performed on samples of Ti-6A1-4V under both cyclic and static loading conditions. The observations were conducted in a specially-designed loading stage in-situ in a scanning electron microscope. SCOD's of cracks as small as 7μ in surface length have been studied with this technique. Preliminary results have indicated that crack opening is

MICRONS

DD FORM 1473 EDITION OF 1 NOV 65 IS OBSOLETE

UNCLASSIFIED

SECURITY CLASSIFICATION OF THIS PAGE *(When Data Entered)*

purely elastic for the strain range studied although a significant residual opening is apparent when no load is applied.

Concurrent with the experimental efforts, an analytical approach has been developed to predict SCOD for both elastic and plastic loading conditions based on crack geometry. The correlation between predicted SCOD values and independent data for macrocracks is excellent. The approach will be modified to account for the influence of an imposed residual stress field and compared to experimental results on microcrack behavior.

FOREWORD

The research reported herein was conducted by Southwest Research Institute of San Antonio, Texas, under Contract N00014-78-C-0674. The report summarizes work accomplished during the period August 1978 through July 1979. Dr. Bruce MacDonald was the ONR Program Manager. The work was conducted under the general supervision of Dr. Gerald R. Leverant, SwRI Project Manager, with assistance from Mr. John E. Hack, who acted as Principal Engineer. Special acknowledgement is due to Dr. David L. Davidson, who conducted the in-situ loading experiments in the SwRI SEM and, along with Dr. James Lankford, offered many pertinent suggestions. The assistance of Messrs. James Barbee and Ronald McInnis in the x-ray stress measurements and in sample preparation was greatly appreciated.

TABLE OF CONTENTS

LIST OF TABLES

v

LIST OF FIGURES

LIST OF FIGURES

LIST OF FIGURES (CONT.)

I. INTRODUCTION

Fatigue cracks in metals generally nucleate at or near a free surface.
Since initial growth rates of microcracks are very low ($\approx 10^{-7}$ in./cycle),
fatigue cracks spend a significant portion of their lifetime in the near-
surface region. Thus, the residual stress state at the surface produced
by common mechanical and thermal processing can have a marked effect on
the fatigue behavior of a material. This report details the initial re-
sults from an ongoing program to quantify the relationship between surface
condition and fatigue microcrack growth.

The aim of the current research is to relate the effects of surface
residual stresses to surface crack opening displacement (SCOD) behavior.
Since COD is directly related to crack growth rate[1,2], this data can
be used to correlate surface residual stress state and fatigue behavior.
A unique loading stage which operates _in-situ_ in an SEM is being used to
generate SCOD vs. load data for microcracks in Ti-6Al-4V. Preliminary re-
sults of experimental observations are presented herein. In addition, the
initial results of an analytical model of SCOD vs. load behavior, based on
crack tip stress intensity, are also presented.

II. DIRECT OBSERVATION OF SCOD VS. LOAD BEHAVIOR

A. Experimental Procedure

The Ti-6A1-4V material used in this study was machined from the rim
portion of a pancake forging that was forged at 1241 K in the α/β phase
field, annealed for one hour at 1227 K, water quenched and then aged at
977 K for two hours. The resultant microstructure, shown in Figure 1,
consisted of primary α particles embedded in a matrix of transformed β
(Widmanstatten α) with an α particle size of approximately 14μm. The
alloy composition is summarized in Table I.

A cantilever beam fatigue specimen was designed to ensure surface
crack initiation. Figure 2 shows the tapered gage section which yields
a constant stress over the entire gage length. It can be seen from the
figure that slots are incorporated in the grip sections to allow for fix-
turing the specimen into the SEM loading stage after the initiation of
cracks in a bending rig.

The SEM loading stage, developed at SwRI[3], is shown in Figure 3.
The stage is capable of cyclically loading a sample in tension-tension
at loads up to 3780 Newtons at frequencies ranging from 0-5 Hz while
maintaining the area of interest within the viewing screen of the SEM
and in focus. Crack behavior can be videotaped and replayed for analysis
of crack opening displacement response. In addition, samples can be
statically loaded in tension at loads up to 4895 Newtons.

Samples were machined and treated to various surface conditions rep-
resenting electropolishing, single point tool machining, shot-peening to
various intensities, and abusive grinding. The non-shot-peened specimens
were subsequently shot peened everywhere but in the gage length to promote
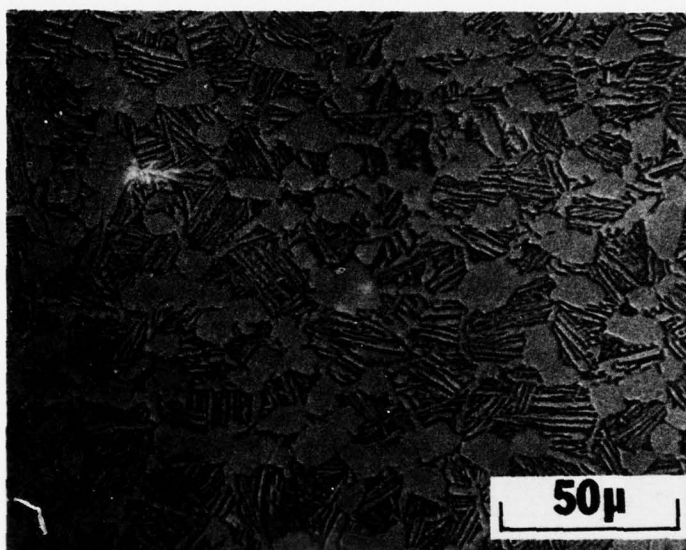
FIGURE 1. THE MICROSTRUCTURE OF THE Ti-6A1-4V MATERIAL USED IN THIS
STUDY. The microstructure was developed by forging at
1241°K, annealing for one hour at 1227°K, water quenching
and aging for 2 hours at 977°K.

TABLE I

RANGE OF ANALYZED COMPOSITIONS FOR Ti-6Al-4V MATERIAL

Element	Wt. Pct.
Al	6.3 - 6.4
V	4.3
Fe	0.10 - 0.18
O	0.17 - 0.18
N	0.013 - 0.015
H	0.005 - 0.006

TABLE II

COMPARISON OF INDEPENDENT X-RAY STRESS MEASUREMENTS ON
A SAMPLE WITH A SLIGHTLY COMPRESSIVE SURFACE RESIDUAL STRESS

Measured Quantity	1st Run		2nd Run	
	Cu K_{α_1} Peak	Cu K_{α_2} Peak	Cu K_{α_1} Peak	Cu K_{α_2} Peak
$\psi=0°$ Peak Position ($°2\theta$)	141.96	142.77	141.94	142.75
$\psi=45°$ Peak Position ($°2\theta$)	142.16	142.93	142.12	142.90
Residual Stress (MPa)	-108.33	-91.77	-98.24	-87.99
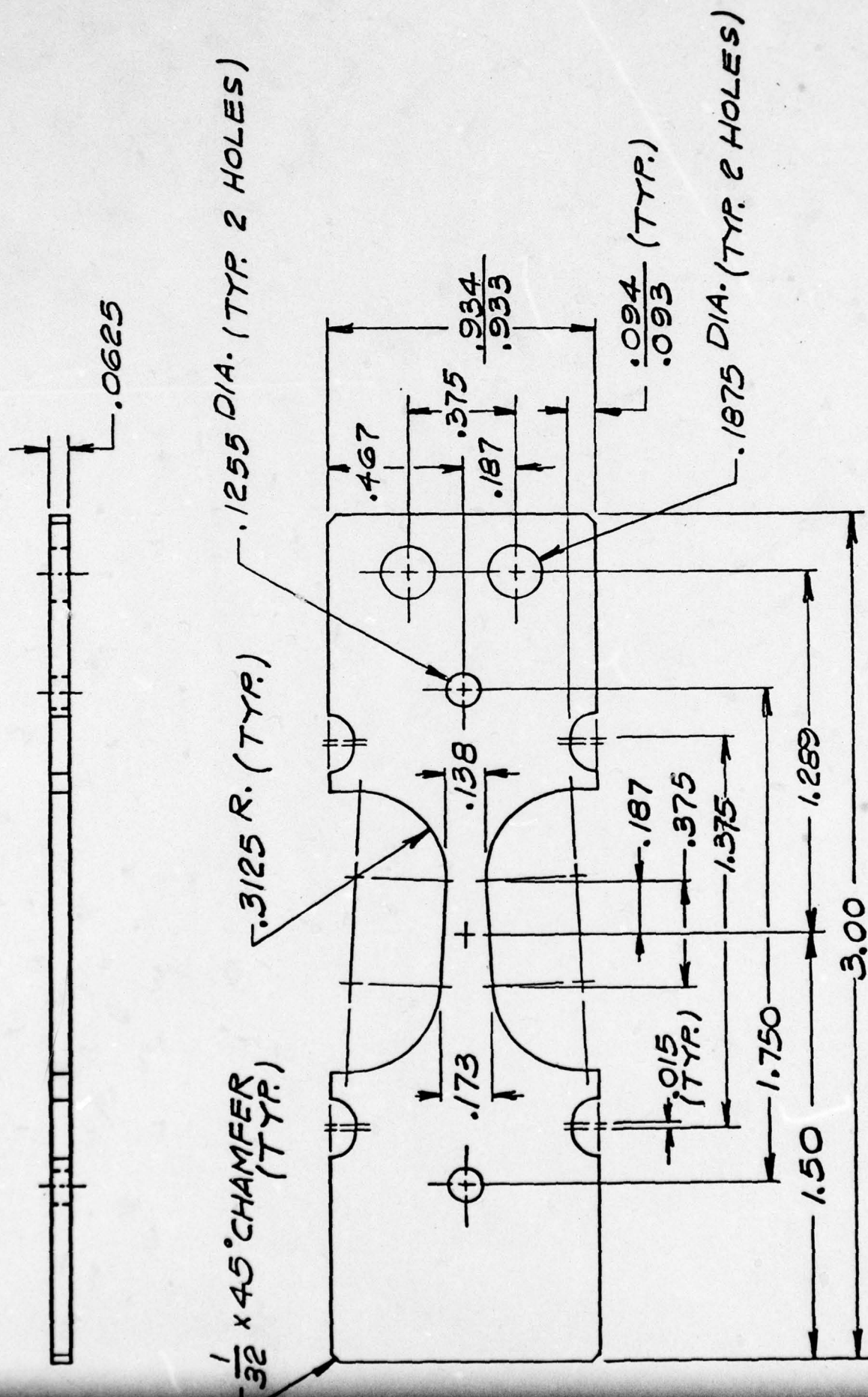
FIGURE 2. CANTILEVER BEAM FATIGUE SPECIMEN

5
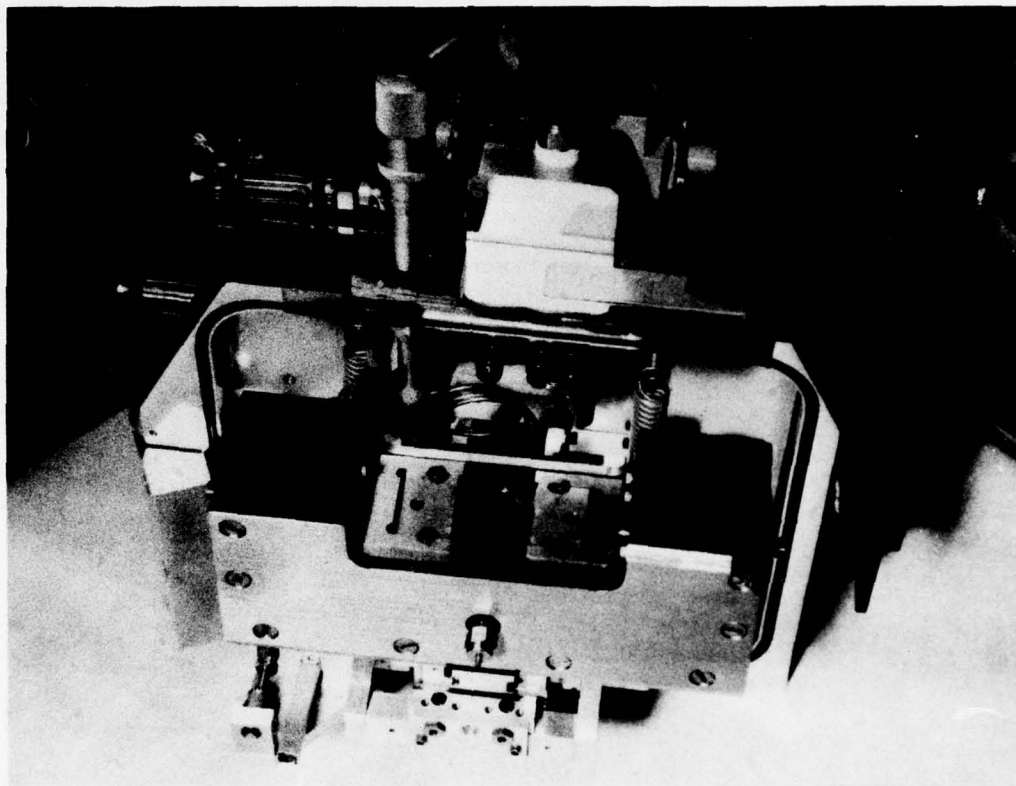
FIGURE 3.   IN-SITU LOADING STAGE FOR SEM.
Carbon/Carbon composite speci-
men is shown loaded in stage.

crack initiation in the gage section. An abusively-ground specimen, Sample 8, was peened over everywhere but a small "window" area approximately 1/8 in. square.

The two exposure x-ray technique[4] was used to measure the surface residual stress on all the samples. A computer program was developed to perform a second degree curve fit on the intensity vs. 2θ data obtained from the x-ray measurements. Enough points are used to define the peaks of interest at $\psi = 0$ and $45°$, then the peak positions, peak shift, and residual stress are calculated. A comparison of measurements on a sample with a slight amount of compressive residual stress, Sample 9, taken at different times under similar conditions showed that the technique was reproducible to within $\pm 0.015°$ for peak positions and ± 5.06 MPa in residual stress (Table II). This is well within the predicted accuracy of the technique.[4]

Cu K_α radiation was used for all measurements in conjunction with a $0.2°$ receiving slit and a $3°$ primary beam slit. The $3°$ primary beam slit was masked with a 127 μ thick α brass foil to restrict the height of the beam impinging on the sample surface to within the thickness of the gage section. No Soller slits were used and the measurements for all peaks were performed with the detector at the focus position for each peak. A Ni filter was used to ensure a strong Cu K_α peak. The [213] plane of α titanium was chosen for the diffracting plane which has a peak at approximately $2\theta = 141°$. The stress constant for these conditions is 5.51 MPa/ $0.01°$ $\Delta 2\theta$.

Results of x-ray residual stress measurements on the gage sections of the prepared specimens are presented in Table III. These values are

TABLE III

RESULTS OF RESIDUAL STRESS MEASUREMENTS

Sample No.	Type	Condition	$2\theta_{\psi=0°}$	$2\theta_{\psi=45°}$	$\Delta 2\theta$	σ_R (MPa)
1	Blank	.011A Shot-Peen	140.90°	142.18°	1.28°	-705.5
2	Blank	.011A Shot-Peen	141.02°	142.22°	1.20°	-661.4
3	Blank	.006N Shot-Peen	141.50°	142.20°	0.70°	-385.8
4	Blank	Single-Pt. Tool-63-AA	141.55°	142.10°	0.55°	-303.2
5	Blank	Single-Pt. Tool-63-AA	141.87°	142.31°	0.44°	-242.5
6	Specimen	Electropolished	142.19°	142.17°	-0.02°	11.0
7	Specimen	.011A Shot-Peen Followed by Slight Mechanical Polish and Electropolish	141.81°	142.24°	0.43°	-238.3
8	Specimen	Abusively Ground (small window)	142.34	142.42	0.08°	-46.8
9	Specimen	Mechanical Polish Followed by Slight Electropolish	141.95	142.14	0.19°	-103.3

uncorrected for beam penetration at the present time. As would be expected, the shot-peened specimens show the highest level of compressive residual stress, while the electropolished specimen has essentially zero surface residual stress. It is believed that the ground surface shows a slight compressive stress because the small window area is surrounded by a much larger area under the compressive residual stress field due to the peening operation. The use of such a small window has been discontinued. Preliminary stress measurements on an abusively-ground specimen with the entire gage section in the as-ground condition indicate a slight tensile residual stress in the specimen.

Samples 6, 7, and 8 were precracked in bending within the strain limits of 0.3 ± 0.5% at 1 Hz. All testing was performed at room temperature. Prior to examination of the SCOD behavior, the samples were "shaken down" by several hundred cycles under load control in axial tension in the SEM loading stage. Load limits used were 100-690 MPa applied at 3 Hz. Both static and dynamic measurements of the SCOD vs. load behavior were performed on the three specimens.

Dynamic observations of the cyclic loading were videotaped for real time measurement of SCOD. However, in the case of Sample 6, motion due to a poor fit in the grips of the loading stage precluded accurate measurements. The sample design was slightly altered to that in Figure 2 for subsequent specimens to avoid this problem.

B.   Results and Discussion

Static observations on Sample 6 (zero residual stress) yielded excellent results. Scanning electron micrographs of the SCOD of a 200 μm long crack at several load steps are presented in Figures 4-8. Measurements of

FIGURE 4.   SEM MICROGRAPH OF SCOD OF SURFACE MICROCRACK IN SAMPLE 6 @ 34 MPa (1000X)

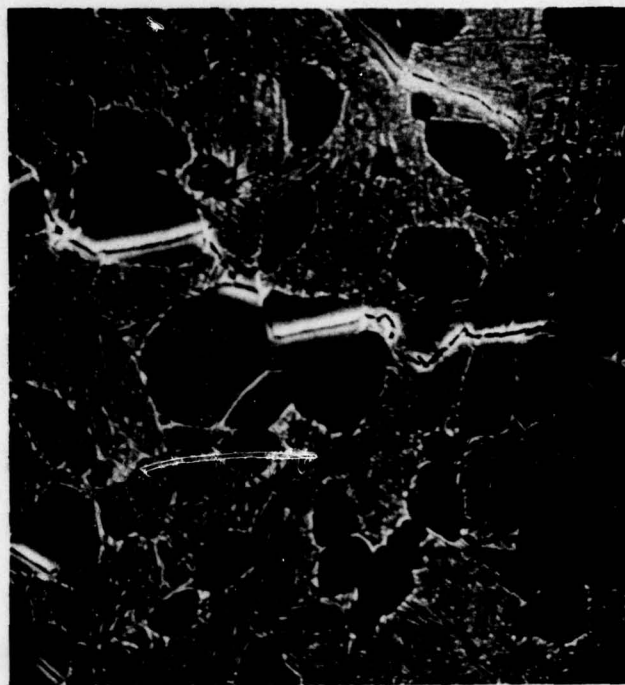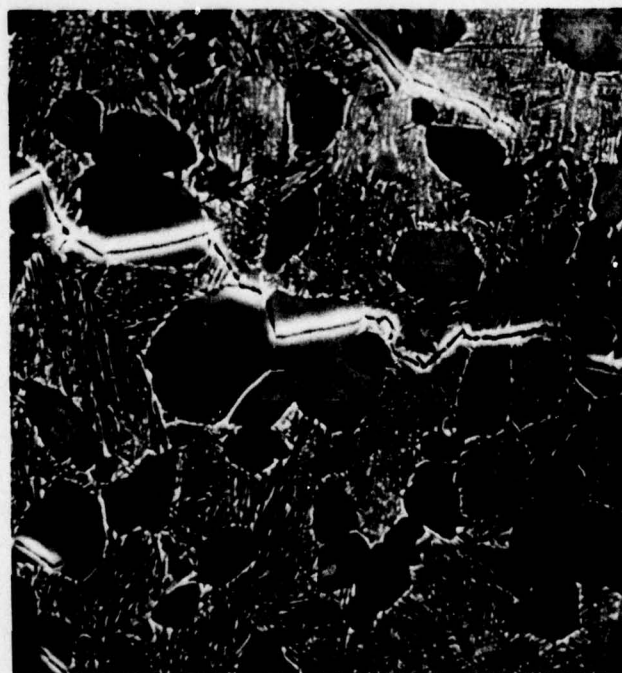FIGURE 5.   SEM MICROGRAPH OF SCOD OF SURFACE MICROCRACK IN SAMPLE 6 @ 276 MPa (1000X)
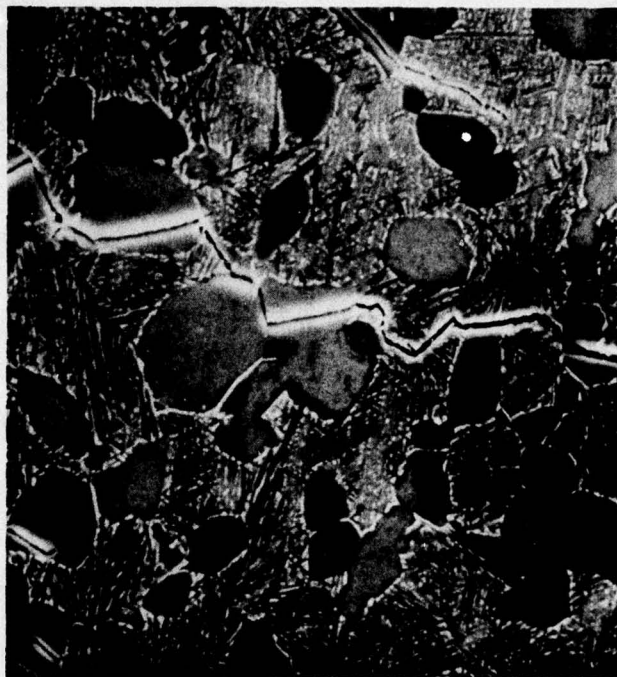
FIGURE 6. SEM MICROGRAPH OF SCOD OF SURFACE MICROCRACK IN SAMPLE 6 @ 551 MPa (1000X)
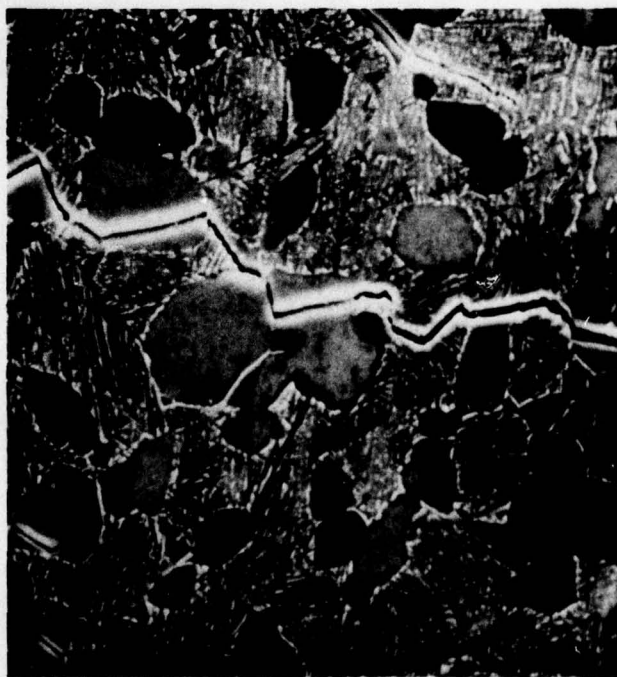

FIGURE 7. SEM MICROGRAPH OF SCOD OF SURFACE MICROCRACK IN SAMPLE 6 @ 792 MPa (1000X)
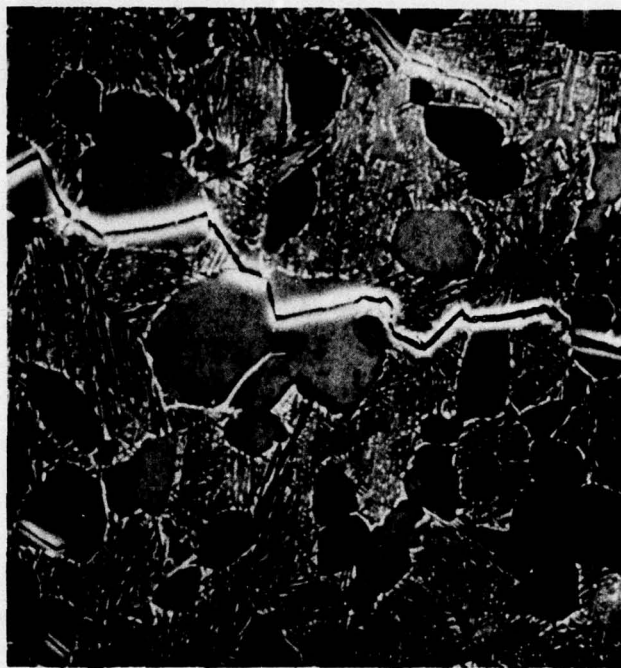
FIGURE 8. SEM MICROGRAPH OF HYSTERESIS IN SCOD OF SURFACE MICROCRACK
IN SAMPLE 6 @ 551 MPa IN UNLOAD CYCLE. Compare with Fig-
ures 6 and 9 (1000X).

SCOD were taken from the micrographs, and the results are plotted against the applied stress in Figure 9. As can be seen from the figure, the SCOD behaves linearly with stress up to approximately 100 ksi and increases rapidly with stress above this level. The unloading plot is also linear with respect to stress and is parallel to the linear portion of the loading curve. No surface crack extension was observed at any time during the course of the SCOD measurements. Thus the method utilized here appears particularly well suited for direct measurements of SCOD under load.

Several points about the plot in Figure 9 are worthy of mention. The first is the rapid rise in SCOD at stress levels above 690 MPa. Room temperature creep of Ti alloys is an established phenomena at high fractions of the yield stress.[5,6] Since the yield stress of α/β forged Ti-6Al-4V is approximately 860 MPa, it is probable that creep localized at the microcrack, or creep combined with extensive local plasticity, is responsible for the hysteresis loop in the SCOD stress behavior. Subsequent experiments were run with a maximum stress of 690 MPa with the result that the deviation from linearity was insignificant.

A second interesting characteristic apparent in Figure 9 is that the SCOD is not zero at zero load even though there was essentially zero residual stress present in the electropolished sample. The lowest stress point measured on the curve was at approximately a 35 MPa preload to avoid putting certain components of the loading stage in tension. Initially, it was not known whether a residual opening was introduced by plastic deformation during the bending cycles or if the crack was wedged open below the surface as a result of mixed mode deformation due to the crystallographic nature of the crack. Subsequent experiments on Samples 7 and 8 indicate that the large residual opening is indeed introduced during the bending cycles.
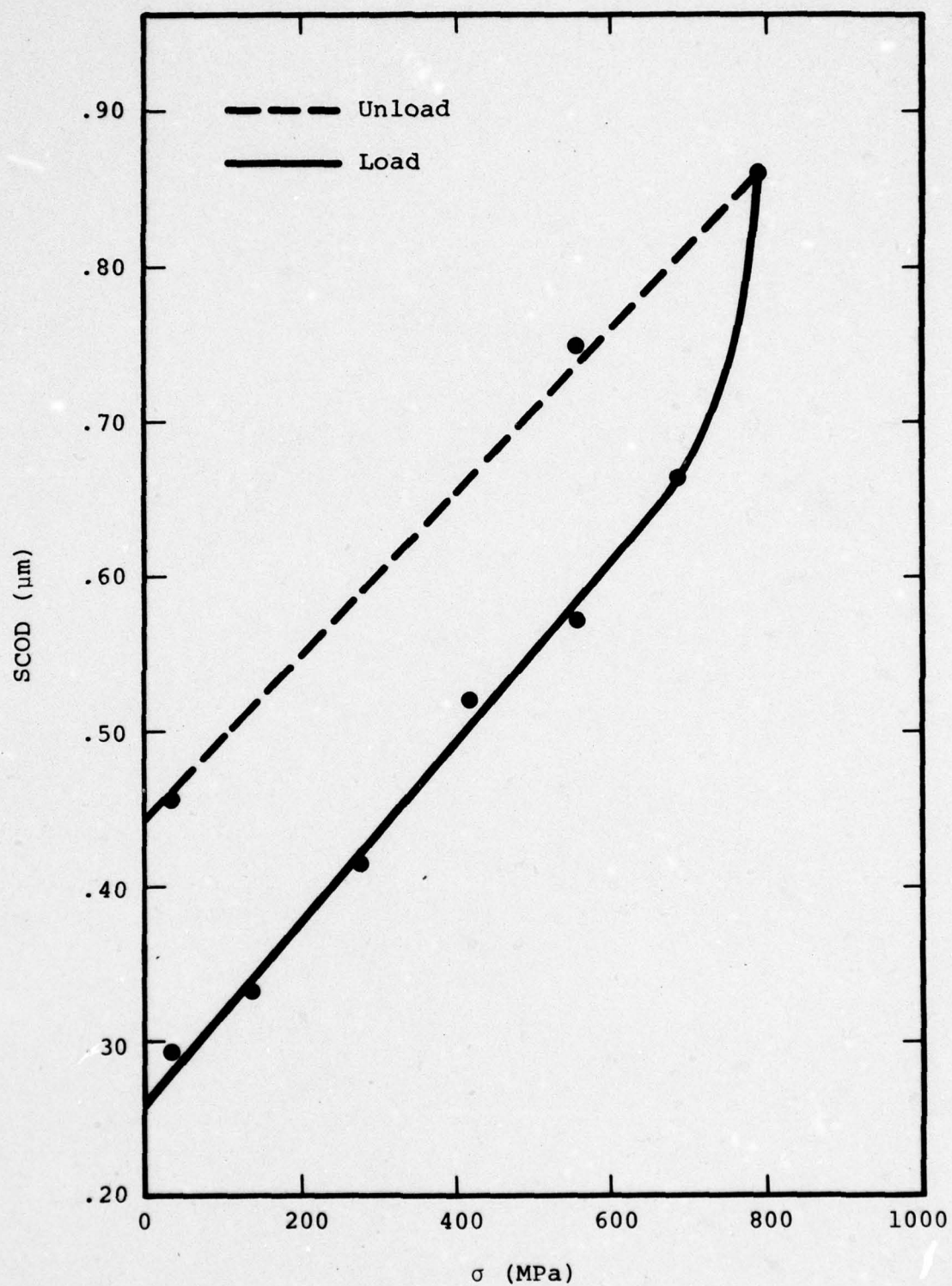
13

FIGURE 9. MEASURED SCOD VS. σ RESPONSE FOR MICROCRACK IN
SAMPLE 6

The linear behavior of the SCOD responses in these experiments appears to preclude any contribution from closure phenomena and shows that the opening is most likely associated with the large strain range employed. The strain range will be reduced in future experiments to lessen this effect.

Similar measurements were performed on five cracks in Sample 7. This sample had been shot-peened to an .011A intensity and subsequently mechanically and electrochemically polished to a smooth finish before precracking. The surface residual stress, as indicated in Table III, was approximately 207 MPa. The cracks used for the measurements are shown in Figures 10-12. As can be seen from the figures, the cracks range in length from 7-125 μ. The residual opening prior to loading in the SEM stage is apparent. Figure 13 is a plot of SCOD vs. load for the three sets of cracks. The three small cracks of Figure 12 are shown in one line because their response was extremely similar. The curves are also normalized to zero by subtracting out the residual opening. Measurements taken from videotaped sequences of cyclic loading agreed very well with static measurements. The curves appear to show a decrease in opening with crack length at a given load. However, the aspect ratios (crack depth/half-crack length) for these cracks are in the process of being determined, so no significance can be attached to the magnitude of the shift at this time.

SCOD measurements have also been performed on several cracks in Sample 8. The cracks on the surface of this specimen are shown in Figures 14-18. Presently, the data are not yet fully analyzed for this case. It should be noted that in all samples many cracks were present. Except in the cases of the cracks shown in Figures 12 and 14, only cracks which were isolated by many crack lengths from other cracks were utilized in

FIGURE 10. SEM MICROGRAPH OF 125 μm LONG SURFACE MICROCRACK USED IN SCOD
MEASUREMENTS ON SAMPLE 7 (1000X)

FIGURE 11. SEM MICROGRAPH OF 90 μm LONG SURFACE MICROCRACK USED IN SCOD
MEASUREMENTS ON SAMPLE 7 (1000X)

FIGURE 12. SEM MICROGRAPH OF GROUP OF CRACKS IN THE RANGE OF 7 μm LONG
USED IN SCOD MEASUREMENTS ON SAMPLE 7 (1000X).
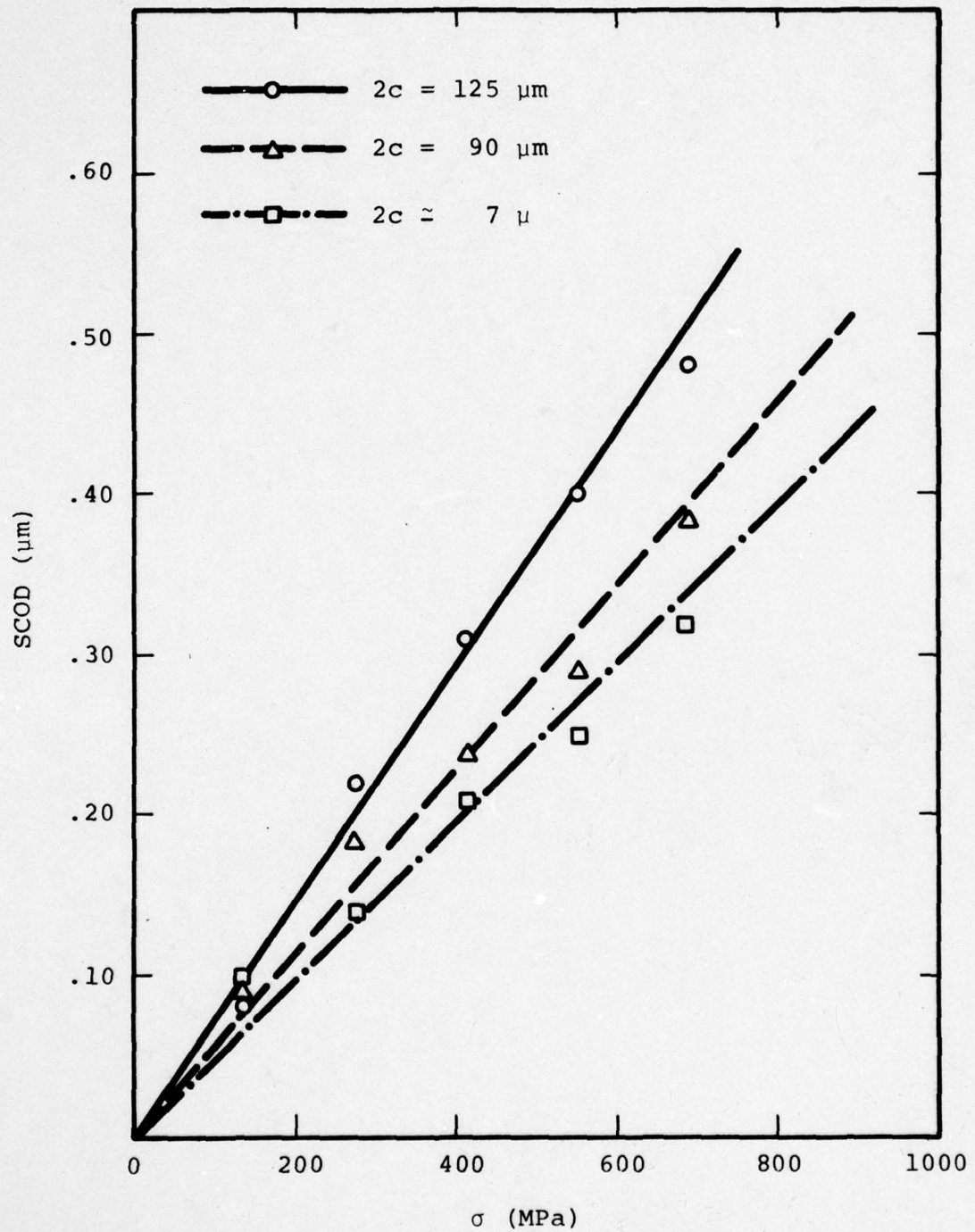
FIGURE 13.   MEASURED SCOD VS. σ RESPONSE FOR MICROCRACKS IN
SAMPLE 7

FIGURE 14.   SEM MICROGRAPH OF SURFACE MICROCRACKS USED IN SCOD MEASURE-
MENTS ON SAMPLE 8.   Labeled Crack 2 (1000X).

FIGURE 15.   SEM MICROGRAPH OF SURFACE MICROCRACK USED IN SCOD MEASURE-
MENTS ON SAMPLE 8.   Labeled Crack 4 (1000X).

20

FIGURE 16.   SEM MICROGRAPH OF SURFACE MICROCRACK USED IN SCOD MEASURE-
MENTS ON SAMPLE 8.   Labeled Crack 5 (1000X).

FIGURE 17.   SEM MICROGRAPH OF SURFACE MICROCRACK USED IN SCOD MEASURE-
MENTS ON SAMPLE 8.   Labeled Crack 6 (1000X).

FIGURE 18.   SEM MICROGRAPH OF SURFACE MICROCRACK USED IN SCOD MEASURE-
MENTS ON SAMPLE 8.   Labeled Crack 7 (1000X).

taking measurements. Also, the largest cracks observed in each case were measured. This was to ensure that the data obtained were a true measurement of SCOD as affected only by load and crack aspect ratio without interference from stress fields from other cracks in the sample.

III. PREDICTION OF SCOD VS. LOAD BEHAVIOR

A.   Analytical Approach

Concurrent with the experimental observations described in the previous section, the development of an analytical model was initiated to allow for the prediction of SCOD behavior under the influence of residual stress. The approach chosen is based on the stress intensity at the surface and subsurface crack tips. Gray[8] gave the closed form stress intensity factors for these two points along the crack front as:

$$K_{Isur} = \sigma\sqrt{\pi a}\ [1+0.12\ (1-\frac{a}{c})][1-0.619\frac{a}{c}\ ]^{1/2}$$

$$K_{Isub} = \sigma\sqrt{\pi \alpha}\ [1+0.12\ (1-\frac{a}{c})]\ \frac{a}{c}\ [1-0.619]^{1/2}$$

(1)

where: K_{Isur} = surface stress intensity in Mode I

K_{Isub} = subsurface stress intensity in Mode I

a   = crack depth

c   = half crack length

as illustrated in Figure 19. The accuracy of these solutions was given by Paris and Sih[9] as +1.5%/-2.5%. In order to obtain the SCOD at the center of the crack, these expressions were combined with the expression given by Broek[10] for the displacement at a Mode I crack in a direction perpendicular to the crack plane:

$$v = 2(1+\nu)\ \frac{K_I}{E}\ \sqrt{\frac{r}{2\pi}}\ \sin\frac{\theta}{2}\ [2-2\nu-\cos^2\frac{\theta}{2}]$$

(2)

where: v   = the displacement in the Y direction

ν   = Poisson's ratio
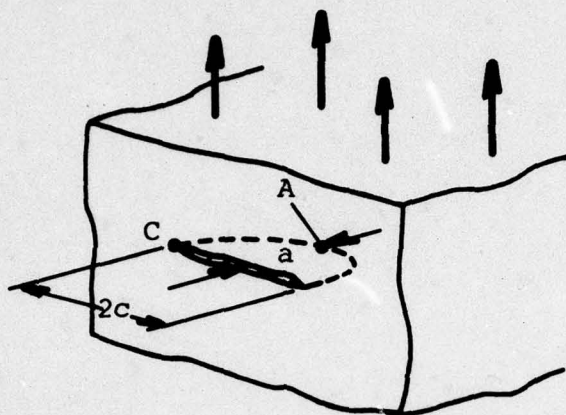
K_I = the Mode I stress intensity factor

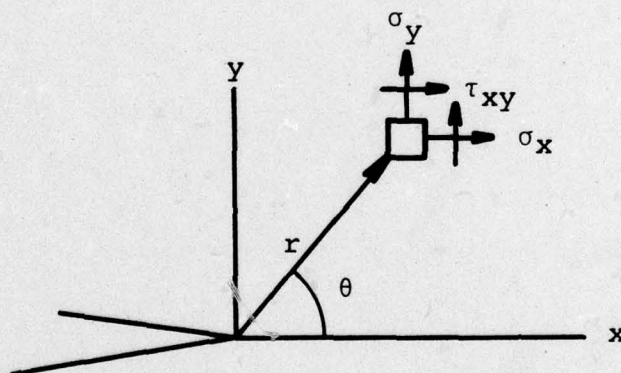FIGURE 19. CRACK GEOMETRY USED IN ANALYTICAL APPROACH

FIGURE 20. COORDINATES OF GENERAL MODE I CRACK SYSTEM

r = distance to point being analyzed

θ = angle between crack plane and point being analyzed with the crack tip as the vertex.

The coordinate system is shown in Figure 20.

It is recognized that Equation (2) is only applicable at distances r small in comparison to the crack length, and that higher order terms must be included if r becomes large. However, the expression will be used to obtain a first approximation to SCOD vs. load behavior for surface cracks and, as will be seen, predictions using such an approach are quite accurate for macrocracks. Solving Equation (2) with $r = a$ (subsurface crack tip) or $r = c$ (surface crack tip) and using the appropriate K_I from Equation (1), one obtains

$$v = 2\sqrt{2} \ (1 - \nu^2) \ \sigma a \ [1 + .12 \ (1 - \frac{a}{c})] \ \sqrt{1 - .619 \frac{a}{c}} \qquad (3)$$

for the displacement at the center of the crack ($\theta = 180°$). The COD is simply twice the displacement or

$$COD = \frac{4\sqrt{2} \ (1 - \nu^2)}{E} \ \sigma a \ [1 + .12 \ (1 - \frac{a}{c})] \ \sqrt{1 - .619 \frac{a}{c}} \ . \qquad (4)$$

B. <u>Results and Discussion</u>

As can be seen from Equation (4), COD behavior for a given material is dependent on the applied stress state and crack geometry. Predictions based on this expression were compared to independent data on macrocracks in Ti-6Al-4V gathered by Collipriest.[11] In his work, Collipriest initiated surface cracks in samples and measured SCOD vs. load until the behavior became extremely nonlinear (i.e., gross plasticity and extension of the crack). Then he fatigued the sample for a short time to mark the end of the first crack extension and repeated his measurements. Table IV summarizes a

TABLE IV

COMPARISON OF PREDICTED SCOD VALUES VS. INDEPENDENT MEASUREMENTS
FOR A SURFACE MACROCRACK IN Ti-6Al-4V

Stress (MPa)	SCOD (calc.) (µm)	SCOD (plas.) (µm)	SCOD (meas.) (µm)
68.9	3.89	3.89	3.81
137.8	7.77	7.80	6.35
206.7	11.66	11.73	10.16
275.6	15.54	15.72	13.97
344.5	19.43	19.76	17.78
413.4	23.32	23.88	20.83
482.3	27.18	28.19	24.89
551.2	30.99	32.51	29.46
599.43	33.81	35.54	34.54
606.32	34.20	35.97	44.70

comparison of SCOD as calculated in the present study [SCOD (calc.)] to that measured by Collipriest [SCOD (meas.)]. As can be seen from the table, the agreement is excellent up to the point where the measured behavior becomes nonlinear.

Equation (4) is totally based on an elastic analysis. As a first approximation for plastic effects, the Irwin plastic zone corrections[12] were applied to Equation (4). With these corrections, a and c were replaced with a' and c', respectively, with

$$a' = a + \frac{(K_{sub})^2}{4\pi \sqrt{2}\, \sigma_y^2}$$

$$c' = c + \frac{(K_{surf})^2}{2\pi\, \sigma_y^2}$$

(5)

where σ_y = yield stress of the material. These corrections allow for plane strain conditions at the subsurface crack tip and plane stress conditions at the surface crack tip.

Predictions based on these corrections are also presented in Table IV as SCOD (plas.). It is obvious that the corrections do not completely make up the difference in the divergence between the calculated and measured results. This is most likely due to the fact that during Collipriest's measurements, crack extension was concurrent with the onset of plasticity. Thus the a/c ratio was increasing while c remained essentially constant (i.e., the parameters in Expression (4) were changing with time after the onset of nonlinear behavior).

Comparison of predicted to measured values after the first crack extension showed good correlation but not as good as with the initial response

shown in Table IV. This is believed to be due to the large amount of plastic strain in the material after the first crack extension. Such data indicates that the proposed model would stand a better chance for success in the present study if the strain and stress ranges used in the precracking and measurement phases of the experimental work are kept well within the elastic range.

No direct comparison of predicted SCOD behavior has been made with actual data generated on this program due to a lack of a/c data on the measured cracks. The determination of these values is in progress and a comparison will be made as soon as they are available. A computer program was written to use Equations (4) and (5) to predict the elastic and plastic SCOD response of the Ti-6A1-4V material used in this program under a variety of combinations of crack length, crack depth, a/c ratio, and stress. For the purposes of the calculations, ν was taken as 0.35, E was set equal to 114 GPa, and σ_y was taken as 861 MPa. A small part of these data is presented graphically in Figures 21-23. Generally, the figures show that, for a given half-crack length and load, SCOD increases as a/c increases (Figure 22); for a given a/c ratio and load, SCOD increases as crack length increases (Figure 23); and for a given a/c ratio and load, SCOD increases as the crack depth increases (Figure 24). Thus, as would be expected, anything which tends to make the crack physically larger also increases the SCOD at a given load. It should be noted that the effect of plasticity in every case is to increase the SCOD over that predicted from a purely elastic analysis. This is due to the increase in effective crack size from the plasticity corrections.
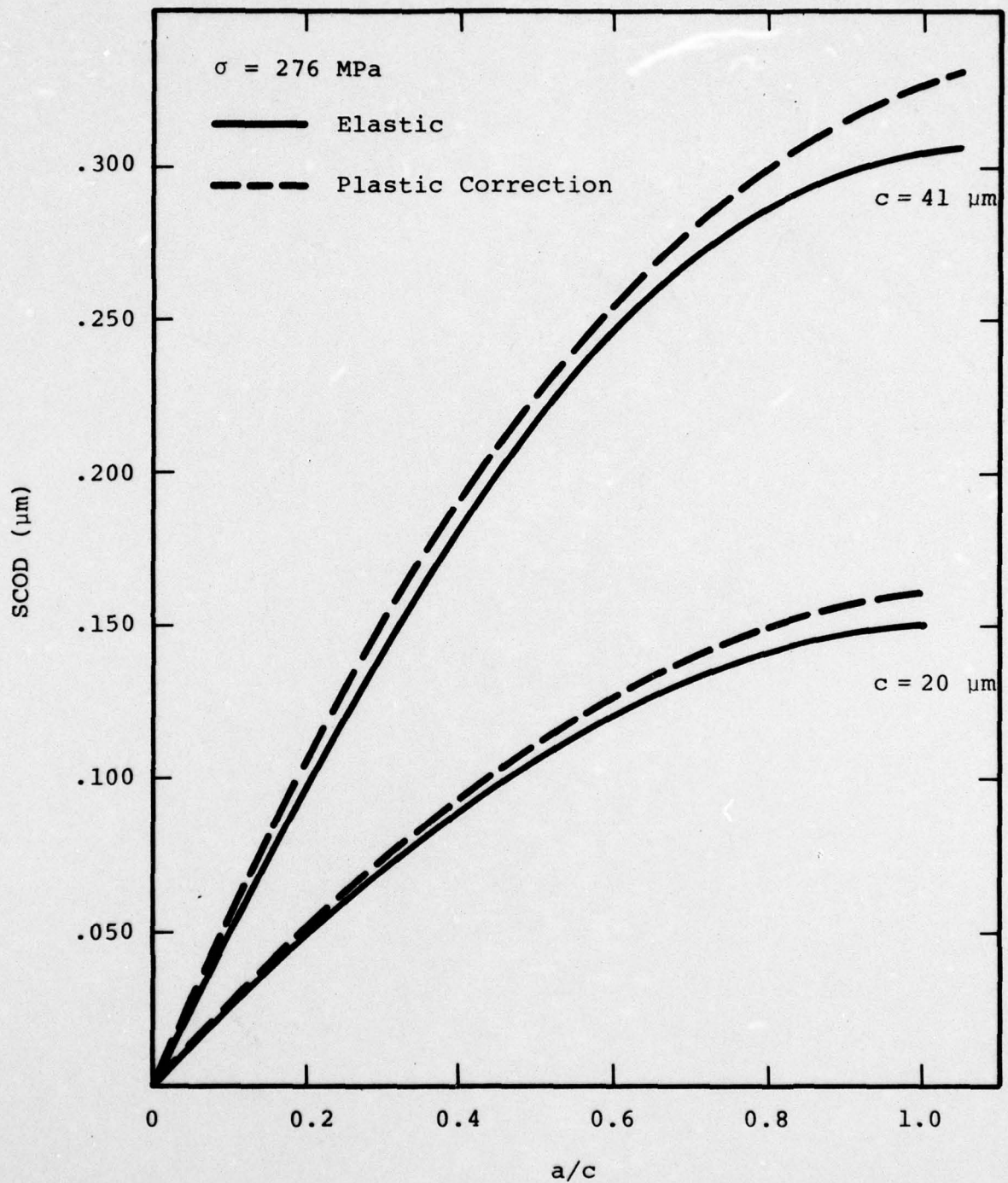
FIGURE 21.   PREDICTED SCOD VALUES AS A FUNCTION OF a/c
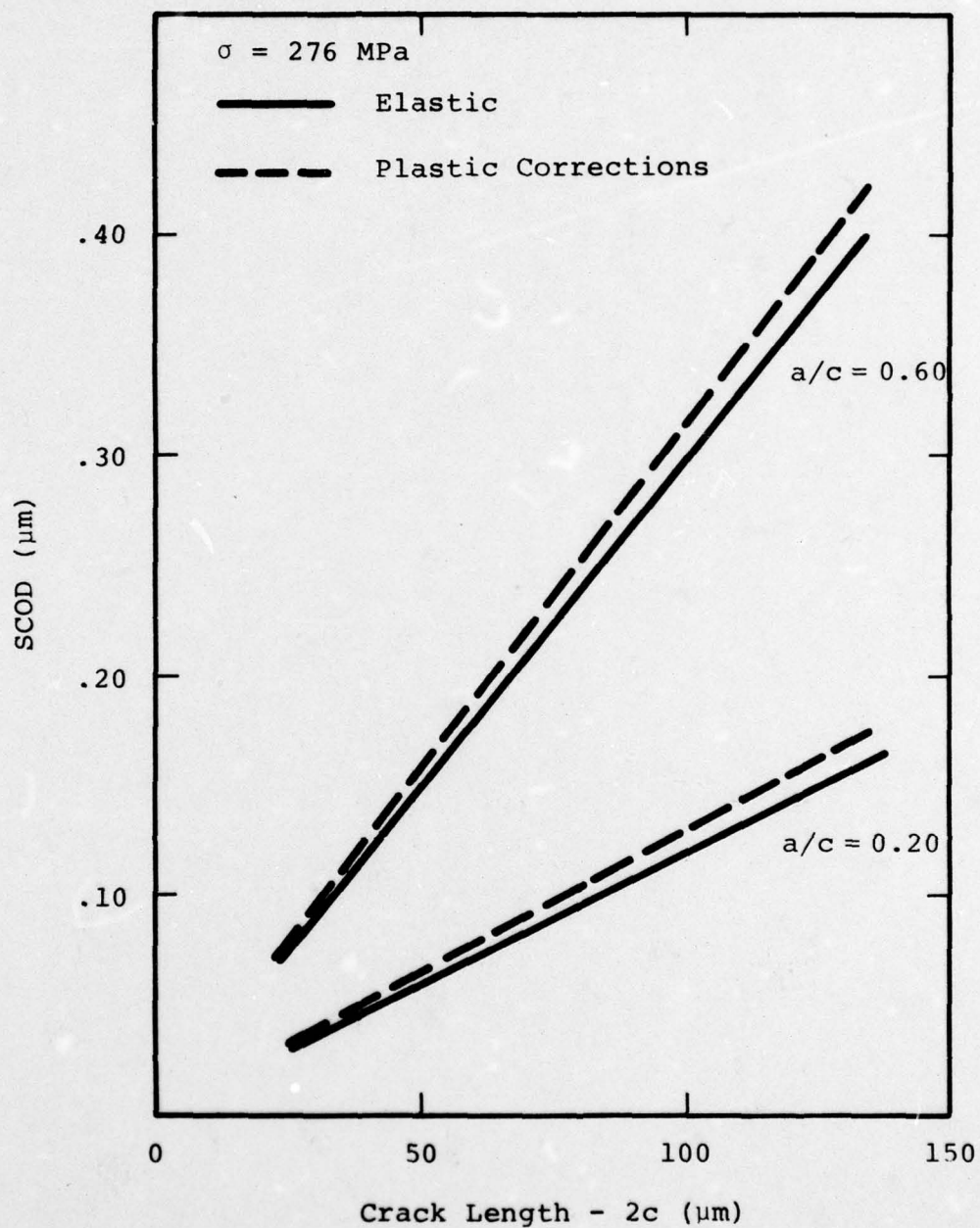
30

FIGURE 22.   PREDICTED SCOD VALUES AS A FUNCTION OF CRACK
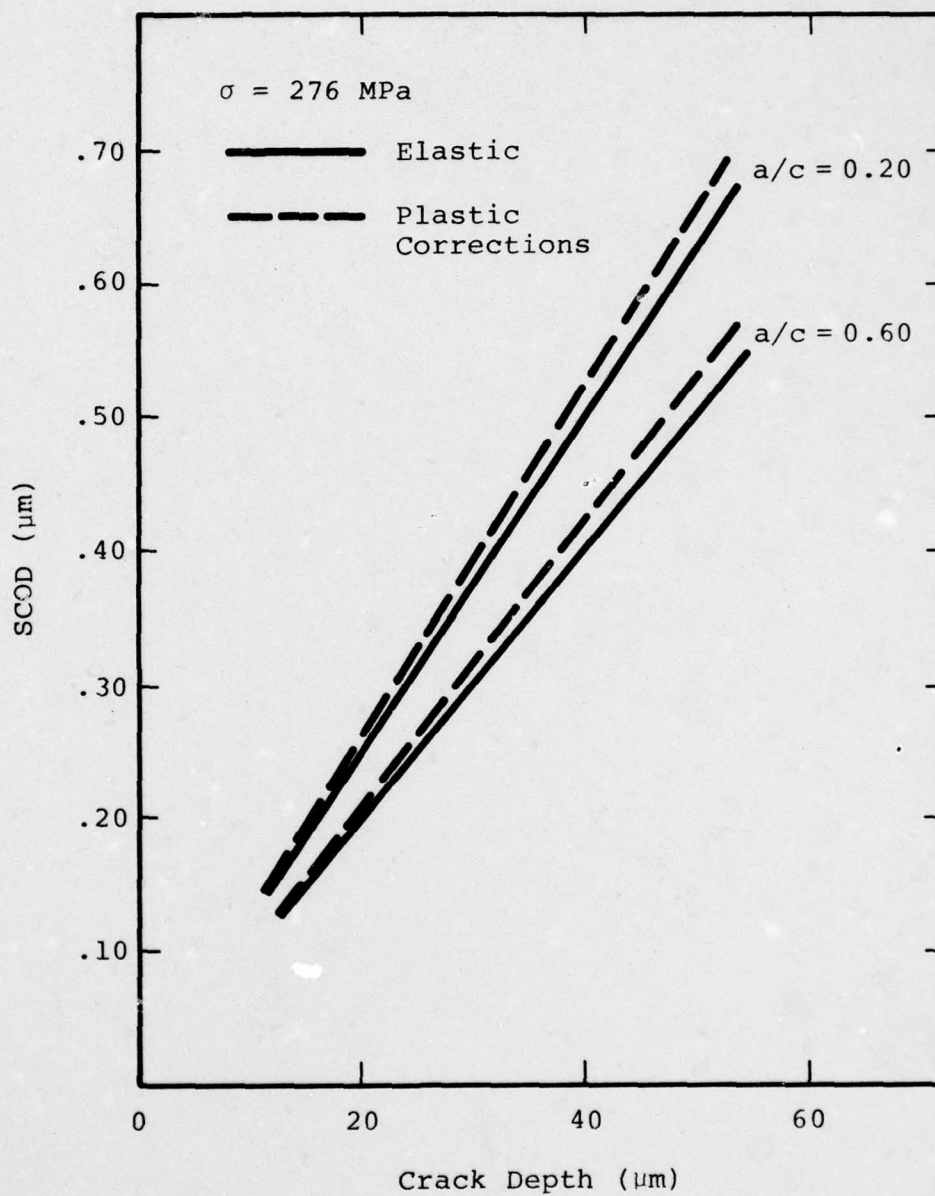   LENGTH

FIGURE 23. PREDICTED SCOD VALUES AS A FUNCTION OF CRACK DEPTH

IV. CONCLUSIONS

1. The use of the _in-situ_ loading stage described herein has proven extremely useful for the direct observation of the SCOD behavior of microcracks (≤ 200 µm).

2. Preliminary results indicate that SCOD vs. load responses of micro-cracks in the Ti-6Al-4V used in this study are linear from zero load until the onset of plastic deformation without any apparent crack closure phenomena occurring.

3. The simple analytical approach developed in this study appears successful in the prediction of the SCOD response of surface macrocracks.

V. REFERENCES

1. A. J. McEvily and T. L. Johnston, *Int. J. Frac. Mech.*, vol. 3, 1967, p. 45.

2. G. G. Garrett and J. F. Knott, *Met. Trans.*, vol. 74, 1976, p. 884.

3. D. L. Davidson and A. Nagy, *J. Phys. E (Sci. Inst.)*, vol. 11, 1978, p. 207.

4. B. D. Cullity, *Elements of X-Ray Diffraction*, Addison-Wesley Publishing Company, Inc., Reading, Massachusetts, 1956, p. 431.

5. G. R. Leverant, G. P. Sheldon, and J. E. Hack, AFOSR Contract No. F49620-78-C-0022, 1978.

6. B. C. Odegard and A. W. Thompson, *Met. Trans.*, vol. 5, 1974, p. 1207.

7. N. Walker and C. J. Beevers, *Fatigue of Engineering Materials and Structures*, vol. 1, 1979, p. 135.

8. T. G. F. Gray, *Int. J. Frac.*, vol. 13, 1977, p. 65.

9. P. C. Paris and G. C. Sih, "Stress Analysis of Cracks," *Fracture Toughness Testing and Its Applications*, ASTM STP 381, American Society for Testing and Materials, 1965, p. 30.

10. D. Broek, *Elementary Engineering Fracture Mechanics*, Noordhoff International Publishing, Leyden, 1974, p. 72.

11. J. E. Collipriest, Jr., "An Experimentalist's View of the Surface Flaw Problem," *The Surface Crack: Physical Problems and Computational Solutions*, ASME, New York, 1972, p. 43.

12. G. R. Irwin, "Plastic Zone Near a Crack and Fracture Toughness," *Proceedings of the Seventh Sagamore Ordnance Materials Research Conference*, 1960, p. iv-63.